Letter

Optics Letters

Temporal pulse quality of a Yb:YAG burst-mode laser post-compressed in a multi-pass cell

Anne-Lise Viotti,[1,2,*] Skirmantas Alisauskas,[1] Henrik Tünnermann,[1] Esmerando Escoto,[1] Marcus Seidel,[1] Katharina Dudde,[1] B. Manschwetus,[1] Ingmar Hartl,[1] and Christoph M. Heyl[1,3,4]

[1]*Deutsches Elektronen-Synchrotron DESY, Notkestraße 85, 22607 Hamburg, Germany*
[2]*Department of Physics, Lund University, P.O. Box 118, SE-221 00 Lund, Sweden*
[3]*Helmholtz-Institute Jena, Fröbelstieg 3, 07743 Jena, Germany*
[4]*GSI Helmholtzzentrum für Schwerionenforschung GmbH, Planckstraße 1, 64291 Darmstadt, Germany*
*Corresponding author: anne-lise.viotti@desy.de

Nonlinear pulse post-compression represents an efficient method for ultrashort, high-quality laser pulse production. The temporal pulse quality is, however, limited by amplitude and phase modulations intrinsic to post-compression. We here characterize in frequency and time domain with high dynamic range individual post-compressed pulses within laser bursts comprising 100-kHz-rate pulse trains. We spectrally broaden 730 fs, 3.2 mJ pulses from a Yb:YAG laser in a gas-filled multi-pass cell and post-compress them to 56 fs. The pulses exhibit a nearly constant energy content of 78% in the main peak over the burst plateau, which is close to the theoretical limit. Our results demonstrate attractive pulse characteristics, making multi-pass post-compressed lasers very applicable for pump–probe spectroscopy at, e.g., free-electron lasers or as efficient drivers for secondary frequency conversion stages.

Ultrafast high-average-power, mJ-class lasers have become essential tools for many scientific and industrial applications within multiple fields including atomic, molecular and optical (AMO) physics, chemistry, material science, or laser machining [1]. While titanium-sapphire-based systems can easily reach pulse durations below 30 fs, they are limited in average power. In contrast, ytterbium (Yb) systems are power-scalable into the kW regime [2,3], as they can easily be diode-pumped but their pulse duration is gain bandwidth-limited to a few 100 fs up to about 1 ps. Many applications, e.g., femtosecond and attosecond science, laser-based particle acceleration, or x-ray free electron laser (FEL) science employing optical pump–probe lasers, would greatly benefit from combining the high average power characteristics of Yb lasers with shorter pulse durations. Nonlinear pulse post-compression methods utilizing spectral broadening followed by chirp removal provide a viable approach to reach this goal. Different techniques have been employed to date including multi-plate continuum generation, multi-pass cells (MPCs), photonic-crystal fiber, and hollow-core fiber-based spectral broadening or self-compression (see [4] and references therein for a complete overview). Despite the large parameter and application range covered by post-compression methods, there is a key challenge that has not attracted much attention until today: the intrinsically limited temporal pulse quality of post-compressed pulses. High order phase contributions from self-phase modulation (SPM) remaining after compression and typical spectral amplitude modulations cause the appearance of pre- and post-pulses or long pedestals, limiting the energy content of the main compressed pulse especially at large compression ratios, and thus restricting the effective peak power boost. In particular, non-optimal compression can affect the temporal contrast. In this context, burst-mode lasers with non-continuous repetition rates employed, e.g., as FEL pump–probe lasers, present additional challenges, as the post-compression process couples input pulse energy instabilities with output pulse parameters. More specifically, such sources can suffer from substantial pulse energy decays within each burst, or similar transient behavior. Precise characterization and control of intra-burst pulse dynamics are therefore crucial.

An important measure for the temporal pulse quality of ultrashort pulses is the temporal contrast, usually quantified as the intensity ratio between satellite pulses and the main pulse. A second important quantity is the relative energy content in the main peak, closely linked to the peak power at a given energy and duration. In high-field physics, such as laser-driven particle acceleration, a high contrast is typically required at long delays (ps to ns regime). Contrast improvement techniques employing, e.g., cross-phase modulation or nonlinear elliptical polarization rotation [5,6], have been employed but reduce the energy in the main peak [7]. Contrarily, for applications such as ultrafast pump–probe spectroscopy at moderate laser intensities, the relative energy content in the pulse with respect to the uncompressed pedestal is of main interest, while relaxed
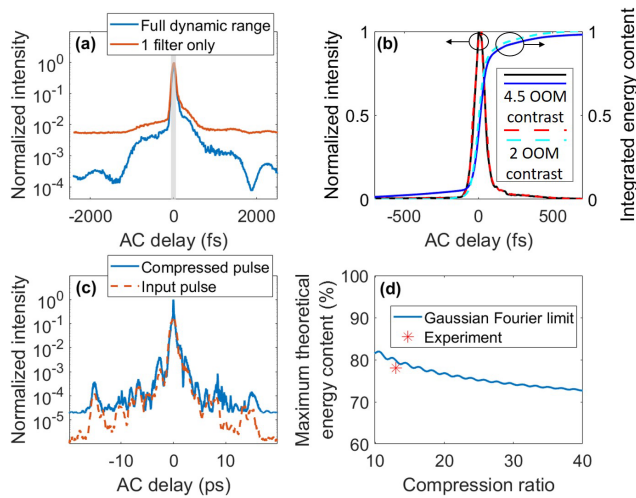
temporal contrast requirements exist. Our efforts therefore address mainly the energy content in the post-compressed pulse.

Reports on pulse post-compression often focus on the full width at half maximum (FWHM) of the pulse duration of the compressed pulse, typically characterized by low-dynamic range autocorrelators (ACs) or second harmonic frequency resolved optical gating (SHG-FROG), while neglecting energy content in the temporal pulse pedestal. This brings along the risk to overestimate pulse energy contrast and peak power. While Pronin *et al.* estimated an energy content of 85% in the main pulse after spectral broadening in a large-mode-area photonic crystal fiber with a compression factor of 14 [8], Köttig *et al.* reported an energy content between 63% and 67% (compression factor of 13.6) using a hollow-core photonic crystal fiber [9]. Up to 80% in the main post-compressed peak was reported with a kW gas-filled MPC for a smaller compression factor of six [10]. Regarding bulk MPCs with compression ratios below 10, estimated energy ratios of 86% [11] and 75% [12] are reported, based on SHG-FROG and AC measurements, respectively. All the above-mentioned energy content estimates were obtained with linear scale measurements.

In this Letter, we investigate the energy content of post-compressed pulses at large compression ratios (>10) employing an Yb:YAG burst-mode laser with a high intra-burst repetition rate (100 kHz) and high average power (320 W in burst), post-compressed in a gas-filled MPC. We characterize individual pulses inside the burst at 100 kHz repetition rate with high dynamic range revealing energy content, spectrum, pulse duration, and phase for individual pulses in the burst. Third-order autocorrelation measurements yield a relative energy content of up to 78% in the main post-compressed pulse as well as a stable broadened spectrum and compressed pulse duration within the flat part of the burst. In contrast to standard characterization methods based on, e.g., AC or SHG-FROG, our method enables a reliable calibration of the pulse energy fraction contained in the post-compressed pulse, yielding a very high energy content for gas-filled MPCs at a large compression ratio.

At the FEL facility FLASH in Hamburg [13], burst-mode lasers matching the temporal structure of the FEL pulse [14] are employed. Recent laser concepts use high average power Yb:YAG lasers together with MPCs for spectral broadening and subsequent pulse compression [15,16], providing simplified solutions compared to traditional optical parametric chirped pulse amplification (OPCPA) approaches. MPCs offer high throughput, large compression ratios [17], good beam quality [12], and great possibilities for average power [10] and pulse energy scaling [18]. In this Letter, we use the FLASH2 burst-mode pump–probe laser [14] with a gas-filled MPC post-compression setup. The laser consists of an Yb laser front-end, which seeds a Yb:YAG Innoslab chirped pulse amplifier (CPA) [18]. Conventionally, the CPA is used as the pump source for an OPCPA system. In our experiment, the output of the amplifier is directly post-compressed [16,17], as depicted in Fig. 1. The system delivers up to 320 W intra-burst average power in 10 Hz burst of about 1 ms length (3.2 mJ single pulse energy at 100 kHz repetition rate) at 1030 nm, with an optimized pulse duration of 730 fs FWHM. The pulses are spectrally broadened in an MPC filled with 1 bar of argon. The cell is used in a near-concentric configuration and consists of two dielectric broadband concave mirrors with radius of curvature of 1 m and a diameter of 100 mm. The MPC is operated with 18 round trips,

Fig. 1. Schematic of the experimental setup. TFP, thin film polarizer; BS, beam splitter; QWP/HWP, quarter-/half-wave plate. The input pulse profile from the Innoslab CPA amplifier (measured via SHG-FROG), the spectrally broadened output of the MPC, and the pulse after the compressor are shown in the blue inset panels and are intensity normalized.

yielding about 87% transmission and good spatial beam quality [16]. A two-lens telescope is used to mode-match the laser beam to the MPC eigenmode. The output of the MPC is compressed using transmission gratings insensitive to polarization in a compact four-pass compressor configuration. Out-coupling of the compressor is performed via a broadband thin film polarizer operating at 70° by adding a $\pi/2$ phase shift in the compressor via double passing a quarter-wave plate. After the compressor, the pulses are sent to a fully automated home-built non-collinear third order AC. A sensitive ultraviolet (UV) photodiode records the full burst trace for each temporal delay in the AC and for several neutral density filters. Individual pulses inside the burst are then extracted by appropriate temporal triggering of our detection system and by stitching the traces obtained with different filters together to form a final AC trace.

For our experiment, the MPC was operated to deliver compressed pulses with a duration of about 56 fs FWHM. Individual pulses inside the MPC compressed output burst are studied first. Figure 2(a) shows the pulse intensity AC trace for the 80th pulse inside the burst recorded employing the full dynamic range of our AC (blue). It is compared in logarithmic scale with a similar measurement at reduced dynamic range performed using a single neutral density filter (orange), illustrating the need for a reliable contrast measurement at higher dynamic range. The corresponding post-compressed individual pulse AC trace is shown in linear scale in Fig. 2(b) for the cases of a reduced dynamic range [two orders of magnitude (OOM)] compared to the full dynamic range obtained with our device (4.5 OOM). Additionally, the integrated energy content computed over the scanning delay reveals that the pedestal at delays prior to -200 fs is completely underestimated for the reduced dynamic rage data. The shaded area in Fig. 2(a) depicts the integration window used for deriving the relative energy content in the compressed peak. We chose twice the FWHM τ of the post-compressed pulse duration and compare the energy content in this window with the energy contained in the 5 ps scanning window. We obtain a relative energy content of 78% in the main compressed pulse, measured via third order AC for a compression ratio of 13 at 320 W in-burst average input power. While the reported result corresponds to a slightly chirped pulse

Fig. 2. (a) Third order AC traces of the 80th post-compressed pulse in the burst in logarithmic scale at full dynamic range (blue) and for a single filter (orange). Integration window (2τ) used for the energy content estimation (shaded area). (b) AC results corresponding to (a) in linear scale and matching integrated energy content. (c) AC trace for a 40 ps scanning window, for the post-compressed pulse (solid line) and MPC input (dotted line). (d) Simulated theoretical limit for the maximum energy content achievable with a FTL post-compressed pulse (solid line) together with the experimental data point (red star).

Fig. 3. Intra-burst dynamics revealing pulse intensity and temporal contrast variations for (a) leading and (b) trailing edges of the burst. (c) Measured relative energy content over the full burst, with a zoom (inset) on the flat part of the burst showing very small variations.

Fig. 4. (a) MPC output pulse energy, showing the burst structure. (b) Full temporal intensity with 10 fs time steps and (c) intra-burst spectra of the full burst of the post-compressed pulses.

(Fourier limit: 52 fs), we achieve a high temporal energy contrast very close to the theoretical limit [red data point in Fig. 2(d)]. Theoretical predictions based on nonlinear pulse propagation simulations [19] considering large compression ratios are also shown in Fig. 2(d). The solid line represents the calculated relative energy content in the main compressed peak for a Fourier transform-limited (FTL) pulse, using the integration window defined above, considering a perfect Gaussian input pulse and linear dispersion-free spectral broadening. Figure 2(c) depicts the AC trace over the full scanning window of the AC setup, i.e., 40 ps, and shows that the pre- and post-pulses have an intensity of less than 0.5% compared to the main peak at time delays longer than 2.5 ps. Peaks at longer time delays are also present in the initial pulse from the Yb amplifier (dotted curve) and, as such, are not inherent to post-compression. The AC traces are recorded with 50 fs (10 fs) steps for the 40 ps (5 ps) scanning window. By normalizing the integrated energy content of the main compressed pulse to the pulse energy, we can easily estimate the peak power. We obtain a peak power boost of around seven, corresponding to a peak power of about 24 GW after post-compression assuming a total setup transmission of 80%. While such a high transmission can easily be reached using gas-filled MPCs in combination with chirped-mirror compressors, the total transmission in our setup was lower due to a grating-based compressor with 56% efficiency.

Using our home-built automated third order AC, we are able to record high dynamic range AC traces resolving all pulses over the full burst, as shown in Figs. 3 and 4. The AC trace resembling the full burst is obtained by combining traces from all individual pulses similar to the blue AC trace in Fig. 2(a). The full AC trace reveals that the pulses are well behaved over the entire flat part of the burst, showing only minor intensity and bandwidth variations in the timing window of 1100–1800 µs, which corresponds to the part of the burst that is overlapped with the FEL
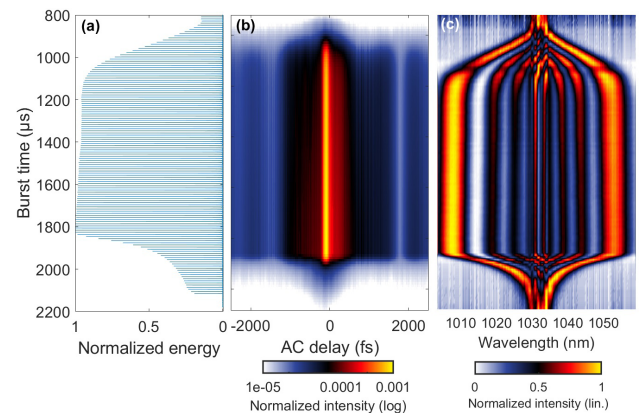
burst in pump–probe experiments. It also reveals fast dynamics at the leading and trailing edges of the burst as shown in Figs. 3(a) and 3(b), caused by a rising (falling) pulse energy resulting in an increasing (decreasing) bandwidth at constant compressor settings, i.e., not all the pulses in burst benefit from an optimal compression. Figure 3(c) shows the relative energy content of the main compressed pulse over the flat part of the burst using again an integration window of 2τ. An energy content of 78% is consistently obtained over a duration of 650 µs, i.e., 65 pulses inside the burst, with a standard deviation below 0.2%.

In Fig. 4(b), the full AC trace is presented along the burst structure [Fig. 4(a)]. Another parameter of particular interest for the MPC output pulses is the broadened spectrum. To measure the spectrum of individual pulses inside the burst, a MHz-rate spectrograph was employed, based on the linear array detector KALYPSO [20,21]. Figure 4(c) presents the resulting spectra for all individual pulses within the burst. Employing our third order AC and the MHz-rate spectrograph allows us to perform intra-burst FROG measurements to retrieve the phase of the individual post-compressed pulses. The approach is similar to the full burst contrast measurement with the UV photodiode being replaced by the fast spectrograph operating with reduced dynamic range compared to the third order AC. The pulses are
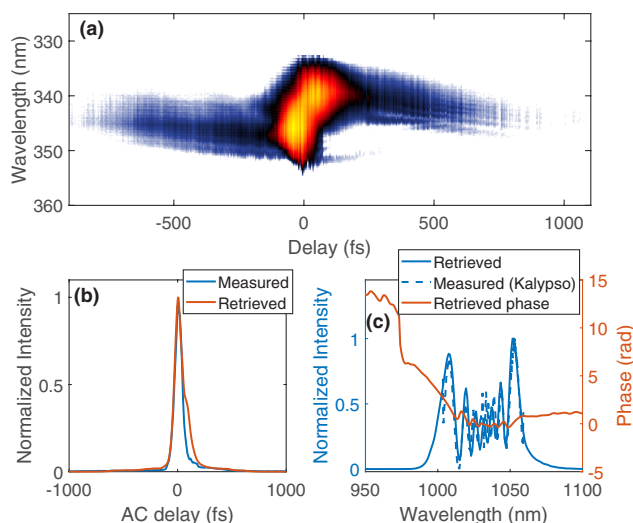
Fig. 5. (a) FROG trace for the 80th pulse in the burst. See Visualization 1 for full burst FROG data. (b) Measured third order AC trace and retrieved pulse for the 80th pulse in the burst. (c) Retrieved and measured MPC spectra, recorded by the MHz spectrograph, corrected for standard silicon response.

retrieved from the third-harmonic FROG traces using a time-domain version of the extended ptychographic iterative engine (ePIE) algorithm, which is commonly used for coherent diffractive imaging [22]. Here, the pulse and its second harmonic are treated as object and probe signals. The two signals are iteratively corrected in the frequency domain using the recorded trace. In the time domain, update functions constructed employing the known mathematical form of the trace are used. Both signals are retrieved separately, coupled by their corresponding update functions. An example of a FROG trace obtained for an individual pulse in the burst is shown in Fig. 5(a). In Fig. 5(b), measured and retrieved pulses are shown with similar durations. Finally, an example of retrieved spectral amplitude and phase is plotted in Fig. 5(c) together with a measured individual pulse spectrum recorded with the MHz-rate spectrograph.

In this work, we have demonstrated reliable intra-burst pulse characterization at 100 kHz repetition rate allowing us to fully resolve spectrum, phase, and temporal contrast of post-compressed pulses from a high power Yb:YAG burst-mode laser. The combination of a high average power Innoslab amplifier with a gas-filled MPC yields 56 fs pulses at millijoule level with a relative energy content of up to 78% in the main pulse. We employed a third order AC, allowing a larger dynamic range than standard characterization techniques to improve the evaluation of the energy content. Stable post-compressed burst parameters are achieved across the entire flat part of the burst. These results demonstrate suitability of the employed MPC post-compression-based laser concept for FEL pump–probe experiments and show promising characteristics for the use of such laser systems as efficient drivers for secondary frequency conversion stages. Moreover, the MHz-rate diagnostic tools presented here will be beneficial for FEL user experiments requiring a high degree of control over the burst dynamics.

Disclosures. The authors declare no conflicts of interest.

Data Availability. Data underlying the results presented in this paper are not publicly available at this time but may be obtained from the authors upon reasonable request.

REFERENCES

1. U. Keller, _Ultrafast Lasers_ (Springer, 2016).
2. M. Müller, A. Klenke, A. Steinkopff, H. Stark, A. Tünnermann, and J. Limpert, Opt. Lett. **43**, 6037 (2018).
3. B. E. Schmidt, A. Hage, T. Mans, F. Légaré, and H. J. Wörner, Opt. Express **25**, 17549 (2017).
4. T. Nagy, P. Simon, and L. Veisz, Adv. Phys. X **6**, 1845795 (2021).
5. N. G. Khodakovskiy, M. P. Kalashnikov, V. Pajer, A. Blumenstein, P. Simon, M. M. Toktamis, M. Lozano, B. Mercier, Z. Cheng, T. Nagy, and R. Lopez-Martens, Laser Phys. Lett. **16**, 095001 (2019).
6. N. Smijesh, X. Zhang, P. Fischer, A. A. Muschet, R. Salh, A. Tajalli, U. Morgner, and L. Veisz, Opt. Lett. **44**, 4028 (2019).
7. A. Jullien, O. Albert, F. Burgy, G. Hamoniaux, J.-P. Rousseau, J.-P. Chambaret, F. Augé-Rochereau, G. Chériaux, J. Etchepare, N. Minkovski, and S. M. Saltiel, Opt. Lett. **30**, 920 (2005).
8. O. Pronin, M. Seidel, F. Lücking, E. Fedulova, M. Trubetskov, V. Pervak, A. Apolonski, Th. Udem, and F. Krausz, Nat. Commun. **6**, 6988 (2015).
9. F. Köttig, D. Schade, J. R. Koehler, P. St. J. Russell, and F. Tani, Opt. Express **28**, 9099 (2020).
10. C. Grebing, M. Müller, J. Buldt, H. Stark, and J. Limpert, Opt. Lett. **45**, 6250 (2020).
11. J. Weitenberg, A. Vernaleken, J. Schulte, A. Ozawa, T. Sartorius, V. Pervak, H.-D. Hoffmann, Th. Udem, P. Russbueldt, and T. W. Hänsch, Opt. Express **25**, 20502 (2017).
12. J. Schulte, T. Sartorius, J. Weitenberg, A. Vernaleken, and P. Russbueldt, Opt. Lett. **41**, 4511 (2016).
13. J. Rossbach, J. R. Schneider, and W. Wurth, et al., Phys. Rep. **808**, 1 (2019).
14. T. Lang, S. Alisauskas, U. Große-Wortmann, T. Hülsenbusch, B. Manschwetus, C. Mohr, J. Müller, F. Peters, N. Schirmel, S. Schulz, A. Swiderski, J. Zheng, and I. Hartl, in _Conference on Lasers and Electro-Optics Europe_ (Optical Society of America, 2019), paper ca_2_1.
15. M. Seidel, F. Pressacco, and O. Akcaalan, et al., "Ultrafast MHz-rate burst-mode pump-probe laser for the FLASH FEL facility based on nonlinear compression of ps-level pulses from an Yb amplifier chain," arXiv:2105.05882v2 (2021).
16. A.-L. Viotti, S. Alisauskas, A. Bin Wahid, P. Balla, N. Schirmel, B. Manschwetus, I. Hartl, and C. M. Heyl, J. Synchrotron Radiat. **28**, 36 (2021).
17. P. Balla, A. Bin Wahid, and I. Sytcevich, et al., Opt. Lett. **45**, 2572 (2020).
18. P. Russbueldt, T. Mans, G. Rotarius, J. Weitenberg, H. D. Hoffmann, and R. Poprawe, Opt. Express **17**, 12230 (2009).
19. M. Hanna, N. Daher, F. Guichard, X. Délen, and P. Georges, J. Opt. Soc. Am. B **37**, 2982 (2020).
20. C. Gerth, G. Brenner, M. Caselle, S. Düsterer, D. Haack, D. Makowski, A. Mielczarek, S. Palutke, L. Rota, V. Rybnikov, C. Schmidt, B. Steffen, and K. Tiedtke, J. Synchrotron Radiat. **26**, 1514 (2019).
21. L. Rota, M. Caselle, E. Brundermann, S. Funkner, C. Gerth, B. Kehrer, A. Mielczarek, D. Makowski, A. Mozzanica, A.-S. Muller, M. J. Nasse, G. Niehues, M. Patil, B. Schmitt, P. Schonfeldt, B. Steffen, and M. Weber, Nucl. Instrum. Methods Phys. Res. A **936**, 10 (2018).
22. P. Sidorenko, O. Lahav, Z. Avnat, and O. Cohen, Optica **3**, 1320 (2016).